Journal of The Electrochemical Society, **161** (12) A1765-A1771 (2014)
0013-4651/2014/161(12)/A1765/7/$31.00 © The Electrochemical Society

Effect of Cation Structure of Ionic Liquids on Anode Properties of Si Electrodes for LIB

Masahiro Shimizu,[a,b] Hiroyuki Usui,[a,b] Kuninobu Matsumoto,[a,b] Toshiki Nokami,[a,b] Toshiyuki Itoh,[a,b,*] and Hiroki Sakaguchi[a,b,*,z]

[a]*Department of Chemistry and Biotechnology, Graduate School of Engineering, Tottori University, Koyama-cho, Tottori 680-8552, Japan*
[b]*Center for Research on Green Sustainable Chemistry, Tottori University, Koyama-cho, Tottori 680-8552, Japan*

Ionic liquids consisted of 1-((2-methoxyethoxy)methyl)-1-methylpiperidinium (PP1MEM) or 1-hexyl-1-methylpiperidinium (PP16) and bis(trifluoromethanesulfonyl)amide (TFSA) were applied to an electrolyte for Li-ion battery. The effect of their cation structure on anode properties of Si electrodes were investigated through the use of thick film prepared by gas-deposition without any binder and conductive additive. The Si electrode in PP1MEM-TFSA exhibited an initial reversible capacity of 2670 mA h g^{-1}, which is larger than that in PP16-TFSA by ca. 900 mA h g^{-1}. Moreover, a comparatively high capacity of 1150 mA h g^{-1} at a high current density of 4200 mA g^{-1} is achieved in PP1MEM-TFSA whereas the Si electrode in PP16-TFSA showed the capacity of only 210 mA h g^{-1}. Raman analysis and electrochemical impedance measurements revealed that PP1MEM cation played a role reducing the interaction between Li ion and TFSA anions, and that Li-ion transfer at the electrode−electrolyte interface in PP1MEM-TFSA was remarkably improved compared with PP16-TFSA. These results indicate that the excellent performances obtained in PP1MEM-TFSA originate from a smooth Li-insertion into Si electrode. It was suggested that introduction of ether functional group into cation is valid to enhance the electrode performance.

Manuscript submitted May 12, 2014; revised manuscript received July 25, 2014. Published August 8, 2014.

Li-ion battery (LIB) has been utilized in large-scale battery systems such as power supply of electric vehicles in recent years. Unfortunately, the conventional LIB using graphite anode has insufficient energy density to satisfy the growing demand. Silicon is one of promising candidates of anode materials for next-generation LIB due to its huge theoretical capacity compared with that of graphite practically used. Si and Li form several Li-rich binary alloy phases such as $Li_{15}Si_4$ at room temperature and $Li_{22}Si_5$ at a high temperature of 415°C, which offers extremely high theoretical capacities of 3580 and 4200 mA h g^{-1}, respectively.[1–3] The volume of Si is, however, significantly changed during alloying/dealloying reactions. The volumetric change ratios per Si atom from Si to $Li_{15}Si_4$ and $Li_{22}Si_5$ correspond to 380% and 410%, which results in a generation of high stress and large strain in the active material. The strain accumulated by repeating charge−discharge cycle causes a disintegration of Si electrodes, leading to a rapid capacity fading and a poor cycle stability. In addition, Si has disadvantages of a low electrical conductivity and a low diffusion coefficient of Li^+ in it (D_{Li+}, 10^{-14} to 10^{-12} cm^2 s^{-1}).[4–6] For these reasons, a practical application of Si electrodes has been hindered. To overcome these problems, considerable attempts have been carried out. Many researchers have studied composite materials consisted of carbon, with mechanically soft property and good electrical conductivity, and pure Si.[7–10] We have recently demonstrated that composite electrodes prepared by using $LaSi_2$/Si and Ni−P/Si exhibit a high anode performance because $LaSi_2$ and Ni−P effectively compensate for silicon's disadvantages.[11–14]

Meanwhile, an electrolyte is also one of the most important factors that determines the battery performance. Room temperature ionic liquids have received intensive attentions as an alternative to conventional organic electrolytes based on carbonate solvents because of their excellent physicochemical properties of high thermal stability, negligible vapor pressure, wide electrochemical window, and high ionic conductivity.[15–18] Nevertheless, there have been a few reports on Si-based electrode in ionic liquid electrolytes.[19–24] Kim et al. prepared $FeSi_{2.7}$ thin-film by using a RF magnetron sputtering, and investigated its electrochemical behaviors in *N*-buthyl-*N*-methylpyrrolidinium bis(trifluoromethanesulfonyl)amide (Py14-TFSA). Although the electrode showed a lower reversible capacity of 760 mA h g^{-1} than that obtained from an organic electrolyte at the first cycle, an excellent capacity retention of 92% at the 100th cycle was achieved in the ionic liquid electrolyte. The reason for the lower initial capacity was suggested to be increase in two kinds of resistance: Li-ion migration in ionic liquid and charge transfer reaction on the electrode.[25] We also demonstrated that the cycle stability of Si-based electrodes are remarkably improved by applying commercial ionic liquids to an electrolyte.[26–28] In the case of using ionic liquid electrolytes, however, charge−discharge (Li insertion−extraction) capacities of Si electrode are tend to be smaller than that in organic electrolytes due to the slower kinetics of Li-ion transfer at the interface between the electrode and the electrolyte. In the TFSA-based ionic liquid electrolytes, Li ion is four-coordinated through the oxygen atoms of two bidentate TFSA anions to form $[Li(TFSA)_2]^-$ ion clusters.[29–31] In addition to this, ionic liquids do not contain any neutral molecules. Therefore, when an electrode is negatively charged, the cations of ionic liquids are accumulated on the electrode surface to compensate the negative charge of the electrode, and the solvated Li-ions ($[Li(TFSA)_2]^-$) exist opposite to the cations in Helmholtz layer, which forms electric double layer at the electrode−electrolyte interface.[32,33] Li-insertion reaction into Si proceeds via several steps: (1) Li-ion migration in the electrolyte bulk, (2) desolvation of $[Li(TFSA)_2]^-$ and Li-ion transport in the electric double layer and/or a solid electrolyte interphase (SEI) layer, (3) alloying reaction of Si with Li, (4) Li diffusion in Si.[34] Among these components, desolvation process is hard to occur by strongly electrostatic interaction between Li ion and TFSA anions, which impedes Li-insertion into Si compared with organic electrolyte system.[25] Charge−discharge capacities are thus limited in the ionic liquid electrolytes system. We consider that if cation of ionic liquid has functionality reducing the interaction between Li ion and TFSA anions, it can enable efficient Li-ion transfer at the electrode−electrolyte interface. As a result, Li-insertion reaction can easily occur, and it can provide the enhancement of charge−discharge capacities of Si electrode. Jung et al. investigated anode properties of graphite electrodes in TFSA-based ionic liquid electrolytes consisted of pyrrolidinium cation with various functional groups by using cyclic voltammetry, and reported that the Li insertion−extraction properties are involved with cation structure of ionic liquids.[35] There has been, however, no study that tried to improve the anode performance of Si electrodes by modifying the cation structure of ionic liquid to the authors' knowledge.

We recently revealed that excellent cycle performanes of Si-based electrodes were achieved in the ionic liquid consisted of piperidinium cation and TFSA anion, and that the electrode performances originate from its high stability against cathodic decomposition.[26–28] TFSA-based ionic liquids show a much higher thermal stability than

*Electrochemical Society Active Member.
[z]E-mail: sakaguch@chem.tottori-u.ac.jp

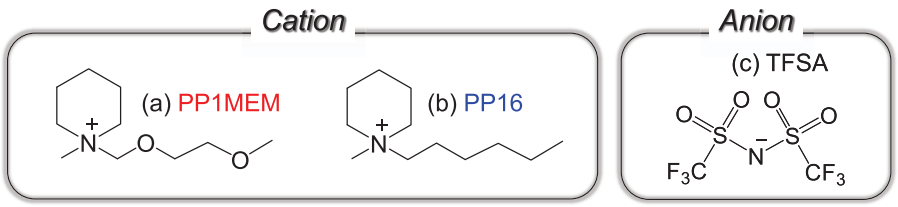

Figure 1. Cation and anion structures of ionic liquids used in this study. (a) 1-((2-methoxyethoxy)methyl)-1-methylpiperidinium. (b) 1-hexyl-1-methylpiperidinium. (c) bis(trifluoromethanesulfonyl)amide.

that obtained from ionic liquids with bis(fluorosulfonyl)amide (FSA) anion, which has a strong advantage in the light of insuring safety of battery.[36] In this study, therefore, we introduced ether group having electron-donating ability into piperidinium cation to reduce the electrostatic interaction between Li ion and TFSA anions by its oxygen atom of local negative charge. For comparison, we also synthesized ionic liquid with alkyl-substituted piperidinium cation having as same chain length as ether-substituted one. In order to directly observe the electrochemical reaction between Si electrode and the electrolyte, Si thick-films prepared by a gas-deposition (GD) method were used. This method does not require any binder and conductive additive to prepare thick-film electrodes.[37,38] It enables us to clarify an original anode property of pure Si electrode. We herein report the effect of cation structure of ionic liquids on anode properties of Si electrodes from the viewpoint of the interaction between Li ion and TFSA anions.

Experimental

Characterization of ionic liquids.— Two kind of ionic liquids were synthesized by organic method as previously reported.[39] Figure 1 shows cation and anion structures of ionic liquids used in this study. One is 1-((2-methoxyethoxy)methyl)-1-methylpiperidinium bis(trifluoromethanesulfonyl)amide (PP1MEM-TFSA). The other is 1-hexyl-1-methylpiperidinium bis(trifluoromethanesulfonyl)amide (PP16-TFSA). All ionic liquids were dried under vacuum at 100°C for 10 h to remove water before analysis described below, and we confirmed water content less than 50 ppm by a Karl-Fisher moisture titrator (Labconco Corporation, FZ-Compact). The viscosity of the ionic liquids was measured by using an E-type viscometer (Visconic ED, TOKYO KEIKI Inc.) under air atmosphere at 303 K. The electrical conductivity was investigated by an electrochemical impedance measurement (CompactStat, Ivium Technologies) through the use of the cell equipped with two Pt electrodes under argon atmosphere at various temperatures from 293 to 353 K. A thermogravimetric (TG) analysis was conducted to determine thermal decomposition temperature of ionic liquids by using a TG analyzer (Thermo plus EVO II, Rigaku Co., Ltd.) with a heating rate of 10°C min^{-1} from ambient temperature to 500°C under argon atmosphere.

Preparation of Si thick-film electrodes.— Si thick-film electrodes were prepared by a gas-deposition method using commercial Si powder (Wako Pure Chemical Industries, Ltd. 99.9%).[26–28] For gas-deposition, a current collector of Cu foil substrate with 20 μm in thickness was set at a distance of 10 mm from nozzle in a vacuum chamber with a guide tube. The nozzle with 0.8 mm in diameter was connected at the end of guide tube. An argon carrier gas with a purity of 99.99% was set under a differential pressure of 7.0×10^5 Pa. After the chamber was evacuated to a base pressure of several ten Pa, an aerosol consisting of the carrier gas and the active material powder was generated in the guide tube, and instantly gushed from the nozzle to the Cu substrate. The weight of the deposited active material on the substrate was measured to an accuracy of 1 μg by ultra-microbalance (XP6, METTLER TOLEDO) equipped with anti-vibration table, and we used Si thick-film electrode in the range of 28−30 μg. Observation by a confocal laser scanning microscope (CSLM, VK-9700, Keyence) revealed that the thickness of Si film is ca. 2 μm.

Evaluation for anode properties of Si electrodes in ionic liquid electrolytes.— We fabricated 2032-type coin cells consisted of Si thick-film electrode as working electrode, Li foil (Rare Metallic, 99.90%, thickness: 1.0 mm) as counter electrode, ionic liquid electrolyte, and propylene-based separator. The areas of the Si thick-film and Li sheet in the cell are 0.5 cm^2 and 1.90 cm^2, respectively. The electrolytes were prepared by dissolving a salt of lithium bis(trifluoromethanesulfonyl)amide (LiTFSA) in each piperidinium-based ionic liquid with a concentration 1.0 mol L^{-1} (M). For comparison, we used an organic-based electrolyte of 1.0 M LiTFSA-dissolved in propylene carbonate (PC; $C_4H_6O_3$, Kishida Chemical Co., Ltd.). The preparation of the electrolytes and the cell assembly were performed throughout in a purge-type glove box (Miwa MFG, DBO-2.5LNKP-TS) filled with argon atmosphere in which oxygen and water were completely removed. The glove box maintained a dew point below −100°C and oxygen content below 1 ppm. Charge–discharge tests were carried out using an electrochemical measurement system (HJ-1001 SM8A, Hokuto Denko Co., Ltd.) in the potential range between 0.005 and 2.000 V vs. Li/Li^+ at 303 K under the constant current density of 0.42 A g^{-1} (0.12 *C*). An electrochemical impedance spectroscopic (EIS) analysis was performed at 0.005 V vs. Li/Li^+ in the frequency of 100 kHz to 10 mHz with amplitude of 5 mV. The surface morphologies of the Si thick-film electrodes after charge–discharge cycle were observed by a field-emission scanning electron microscope (FE-SEM, JSM-6701F JEOL Co., Ltd.). An analysis of the interactions between Li ion and TFSA anions in each ionic liquid electrolyte were conducted by a Raman microscopy system (NanofinderFLEX, Tokyo Instruments, Inc.) with 532 nm line of Nd:YAG laser at room temperature.

Results and Discussion

The physicochemical properties of piperidinium-based ionic liquids synthesized in this study are summarized in Table I. PP1MEM-TFSA exhibited approximately half viscosity compared with that of PP16-TFSA, which means that a coulombic interaction between the dissociated cation and anion was weakened by its ether functional group in PP1MEM cation. It is well known that introducing of alkoxy group having electron-donating ability into quaternary ammonium cation reduces viscosity of ionic liquids.[40–42] Consequently,

Table I. Summary of physicochemical properties of TFSA-based ionic liquids synthesized in this study. The electrolytes were prepared by dissolving of LiTFSA with a concentration of 1.0 M.

Cation	M.W.[a]	η[b]/mPa s	σ[c]/mS cm^{-1} (neat)	σ[c]/mS cm^{-1} (electrolyte)	T_{dec}[d]/°C
PP1MEM	468	69	2.3	0.7	285
PP16	464	132	0.8	0.4	415

[a]Molecular weight.
[b]Viscosity at 303 K.
[c]Conductivity at 303 K.
[d]Thermal decomposition temperature (10% weight loss).

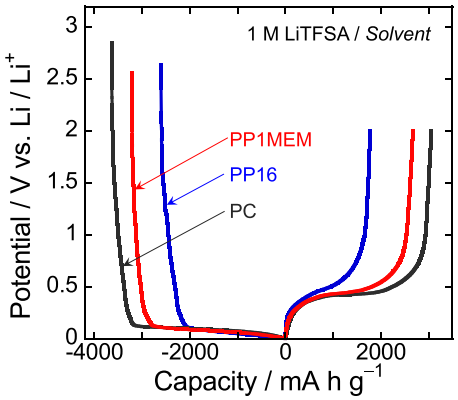

Figure 2. Initial charge–discharge curves of Si thick-film electrodes in ionic liquid electrolytes with cations of PP1MEM and PP16, and in organic-based electrolyte of PC.

in PP1MEM-TFSA system, the higher conductivities were obtained from not only neat ionic liquid but also the electrolyte. The two kind of ionic liquids showed no decomposition at least up to 250°C, though the weight loss of PP1MEM-TFSA was detected at a lower temperature in comparison with PP16-TFSA. The high thermal stability of these ionic liquids is superior to organic solvents, which can enhance the safety of LIB.

Figure 2 shows the first charge−discharge (Li insertion−extraction) curves of Si thick-film electrodes in the piperidinium-based ionic liquid electrolytes and organic electrolyte using PC. In every case, potential plateaus were observed at around 0.1 and 0.4 V vs. Li/Li^+ on charge−discharge curves, indicating alloying and dealloying reactions of Si with Li. In PC, the initial charge and discharge capacities were 3640 and 3060 mA h g^{-1}, respectively, with the first coulombic efficiency of 84%. The irreversible capacity is attributed to a formation of surface layer induced by a reductive decomposition of electrolyte, and the surface layer is mainly consisted of organic and inorganic compounds such as lithium alkyl carbonates ($ROCO_2Li$) and lithium carbonate (Li_2CO_3).[43] By contrast, Si electrode in PP16-TFSA showed the relatively small discharge capacity of 1780 mA h g^{-1}. The initial charge capacity based on Li−Si alloying reaction can be estimated to be about 2070 mA h g^{-1} from range of Li-insertion plateau between 0.005 and 0.120 V vs. Li/Li^+. This capacity corresponds to 58% of the silicon's theoretical capacity (3580 mA h g^{-1}). It is consider that the low utilization of Si is caused by slow kinetics of Li-ion transfer at the interface between the electrode and the electrolyte.[25,27] In the TFSA-based ionic liquid electrolytes, Li-ion is four-coordinated through the oxygen atoms of two bidentate TFSA anions.[29–31] The strongly electrostatic interaction between Li ion and TFSA anions impedes Li-insertion reaction into Si, which causes the decrease in discharge capacity as well as charge capacity as in the PP16-TFSA. It was noteworthy that the discharge capacity of 2670 mA h g^{-1} was achieved in PP1MEM-TFSA. An important point to be emphasized is that the capacity was much higher than that in PP16-TFSA by ca. 900 mA h g^{-1} though these ionic liquids consist of the same anion of TFSA. To evaluate reproducibility, the performances were measured for another electrodes. The standard deviations in the first discharge capacities for PC, PP1MEM-TFSA, and PP16-TFSA are 3058 ± 0.850 mA h g^{-1}, 2681 ± 7.95 mA h g^{-1}, and 1887 ± 106 mA h g^{-1}, respectively. Although the standard deviation in PP16-TFSA is larger than that in PP1MEM-TFSA, a superiority of PP1MEM-TFSA is evident. This result indicates that introducing of ether functional group into cation is valid to exert the high theoretical capacity of Si. We thought that the initial large capacity in PP1MEM-TFSA was presumably due to a smooth Li-ion transfer at interface between the electrode and the electrolyte.

In order to investigate electrochemical behaviors of Li-ion at the interface, an electrochemical impedance measurements were conducted in the frequency range of 100 kHz to 10 mHz. Figure 3 displays Nyquist plots of Si thick-film electrode charged at 0.005 V vs. Li/Li^+ in each electrolyte. In all of the Nyquist plots, it was observed two semicircles and a straight line with a slope of approximately 45° in high frequency region and low frequency region, respectively. The first semicircle denotes interfacial resistance (R_{if}), and is associated with interfacial Li-ion transfer processes that includes desolvation of $[Li(TFSA)_2]^-$, Li-ion transport in electrical double layer and/or a surface layer induced by the decomposition of electrolyte.[24] The second semicircle corresponds charge transfer resistance (R_{ct}), and is related to the process of Li−Si alloying reaction.[34] The straight line in the low frequency named as Warburg impedance (Z_w) is derived from solid-state diffusion of Li in Si.[28] Resistances of these components were analyzed by using an equivalent circuit shown in Figure 3a. We do not discuss here a component of surface layer because it is still a debatable point. The interfacial resistances (R_{if}) in PP1MEM-TFSA and PP16-TFSA were 90 Ω cm^2 and 230 Ω cm^2, respectively, and respective charge transfer resistances (R_{ct}) were 130 Ω cm^2 and 200 Ω cm^2. Both the resistance values in PP1MEM-TFSA were lower than those obtained in PP16-TFSA as expected. In particular, interfacial resistance in PP1MEM-TFSA was less than half of that in PP16-TFSA, indicating a smooth Li-ion transfer at the electrode−electolyte interface. It

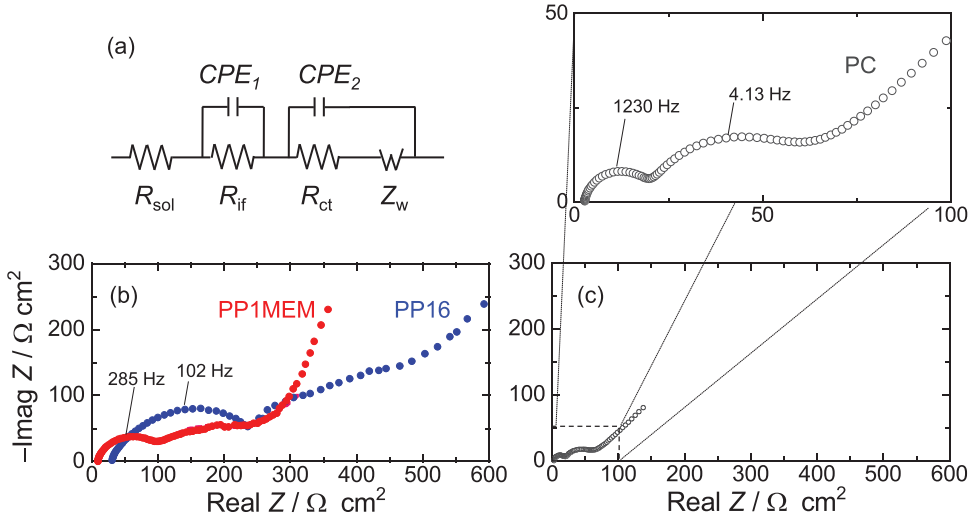

Figure 3. (a) Equivalent circuits for impedance analysis in this study. Nyquist plots of Si thick-film electrodes charged at 0.005 V in (b) PP1MEM-TFSA and PP16-TFSA. For comparison, the Nyquist plots in (c) PC was also plotted.

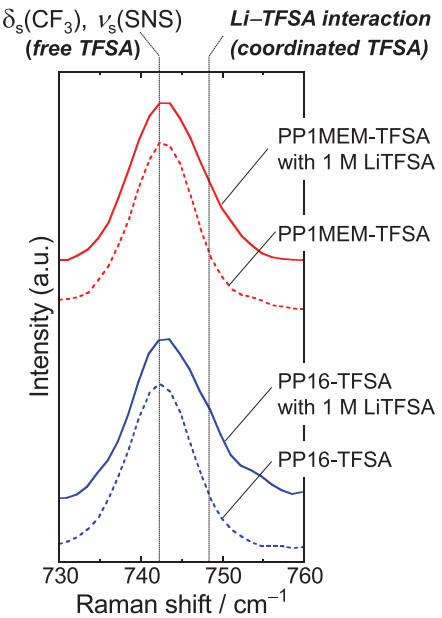

Figure 4. Raman spectra of ionic liquids and the electrolytes consisted of the piperidinium-based ionic liquids and LiTFSA in the frequency range of 730 to 760 cm^{-1}. The cations of ionic liquids are PP1MEM (upper) and PP16 (lower), respectively.

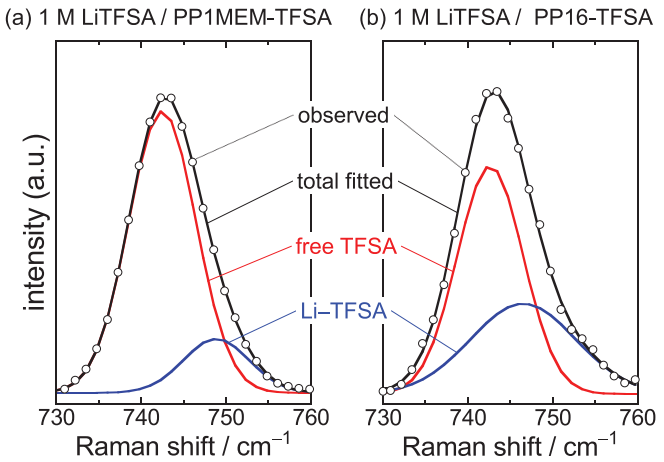

Figure 5. Decomvoluted Raman bands of 1.0 M LiTFSA-dissolved in (a) PP1MEM-TFSA and (b) PP16-TFSA. The dotted, black, blue, and red lines show the observed spectrum, the total Raman spectrum, the deconvoluted components of free TFSA anion and coordinated TFSA anion (Li-TFSA).

was speculated that the charge transfer resistance in PP1MEM-TFSA reduced as a result of improving the Li-insertion into the Si electrode. In the case of using PC, the interfacial resistance and charge transfer resistance became the smallest value among the three kind of electrolytes. These lower resistances originate from weaker interaction between Li ion and solvent molecules in organic electrolyte compared with the electrostatic interaction between Li ion and TFSA anions in ionic liquid electrolyte system. The magnitude of charge and discharge capacities in each electrolyte depends on the values of the respective interfacial resistances. From the results of EIS measurements, we thought that the smooth Li-ion transfer in PP1MEM-TFSA is owing to the reduced interaction between Li-ions and TFSA anions in comparison with PP16-TFSA.

To investigate the interactions between Li ion and TFSA anions in each ionic liquid electrolyte, Raman spectroscopic measurements were carried out. Figure 4 compares Raman spectra for the neat ionic liquids and the electrolytes containing LiTFSA with a concentration of 1.0 M in the frequency range of 730 to 760 cm^{-1}. The intense bands were observed at 742 cm^{-1} in all cases, which is ascribed to the CF_3 bending vibration δ_s (CF_3) coupled with the S−N stretching vibration ν_s (S−N−S) of the TFSA anion.[44–46] This band is assigned to "free" TFSA anions, where Li ion is not coordinated by TFSA anions. In other words, it means the interaction between dissociated cation and TFSA anion in ionic liquid. On the other hand, it is well known that the band position of 742 cm^{-1} showing the interaction shifts to 748 cm^{-1} by coordination of TFSA anions to Li ion.[29,31,47] For electrolytes containing LiTFSA, we can confirm shoulders at around 748 cm^{-1} in the Raman spectrum of each ionic liquid electrolyte. In addition, the shoulder in the PP1MEM-TFSA was obviously smaller than that observed in PP16-TFSA, which suggests that the interaction between Li ion and TFSA anions in PP1MEM-TFSA is less than that in PP16-TFSA. In order to exactly explore the interactions in each electrolyte, their Raman spectra were separated into the two components including uncoordinated TFSA anions (free TFSA) and coordinated TFSA anions (Li−TFSA) by deconvolution processing as shown in Figure 5. Comparing the intensity ratios of coordinated TFSA that interacts with Li ions, the relative ratio of Li−TFSA interaction in PP1MEM-TFSA system was smaller than that PP16-TFSA system. Kunze et al. have studied an interaction in mixture of LiTFSA and pyrrolidinium-based ionic liquid with cation having alkyl side chain or ether side chain by Raman spectroscopic measurement and nuclear magnetic resonance analysis.[48] According to this literature, less than two anions are required for the coordination of Li ion in 1-(ethoxymethyl)-1-methylpyrrolidinium bis(trifluoromethanesulfonyl)amide (Pyr1[2O1]-TFSA) whereas more than two TFSA anions are necessary to solvate Li ion in the 1-butyl-1-methylpyrrolidinium bis(trifluoromethanesulfonyl)amide (Pyr14-TFSA). The coordination number of TFSA anions to Li ion are 1.55 and 2.12, respectively. This result indicates that the Li−TSFA interaction can be weaken by introducing of ether functional group into cation of ionic liquid, and agrees with our results of Raman measurements. The intensity ratios of Li−TFSA to uncoordinated TFSA (free TFSA) in PP1MEM-TFSA and PP16-TFSA are 0.19 and 0.34, respectively, which suggests that the coordination number of TFSA anions to Li ion in PP1MEM-TFSA is less than two, and smaller than that in PP16-TFSA. Although the total charge of PP1MEM cation is +1.0, the oxygen atoms in the cation are negatively charged due to its electron-withdrawing nature. We therefore consider the effect reducing the interaction between Li ion and TFSA anions by PP1MEM cation originates from the two oxygen atoms in the cation structure. Possible reasons for the small coordination number in PP1MEM-TFSA are one or more of the following: (i) a repulsive force due to electrostatic interaction between TFSA anion and local negative charge of oxygen atoms in the PP1MEM cation, (ii) an attractive force due to electrostatic interaction between an isolated Li ion and the oxygen atoms, (iii) an attractive electrostatic interaction between Li ion binding with TFSA anion and the oxygen atoms. However, it is thought that Li ion in TFSA-based ionic liquid electrolytes is preferentially solvated by TFSA anions owing to a very strong interaction between Li ion and TFSA anion.[49] In addition, the results of Raman measurements for the ionic liquid electrolytes shows the fact that the interaction between Li ion and the oxygen atoms of PP1MEM cation coexists with the interaction between Li ion and TFSA anion, which is probably in a competitive relationship. Tsuzuki et al. have studied the an interaction of LiTFSA complex with *N*,*N*-diethyl-*N*-methyl-*N*-2-methoxyethylammonium (DEME) cation and DEME-TFSA by ab initio molecular calculations.[50] Interaction energy potentials (E_{int}) calculated for DEME-Li systems in various geometries are always repulsive though the potential has a local minimum when the Li ion approaches the oxygen atom in DEME cation with a distance of 2.0 Å, which shows that an isolated Li ion does not form the stable complex with DEME cation. Meanwhile, the potential calculated for DEME−LiTFSA complex has a minimum in a similar way to the DEME-Li system when the Li···O distance

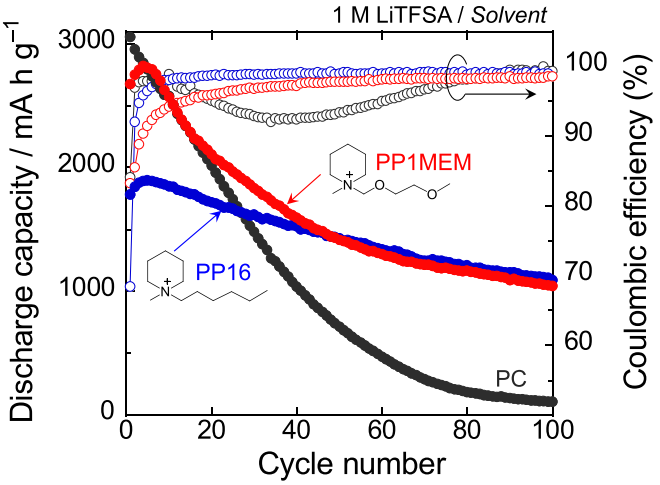

Figure 6. Dependence of discharge (Li-extraction) capacities and coulombic efficiencies on cycle numbers for Si electrodes in PP1MEM-TFSA and PP16-TFSA. For comparison, the performance in PC was also plotted.

is 2.0 Å. E_{int} of fully optimized geometry of the DEME-LiTFSA complex at the HF/6-311G** level is −18.4 kcal mol^{-1}. Furthermore, they calculated an interaction between DEME-TFSA and LiTFSA complex in view of a bulk ionic liquid environment, and reported that its E_{int} (−23.2 kcal mol^{-1}) for most stable orientation is substantially larger than that for the DEME−LiTFSA complex. Based on the results of ab initio calculations, we consider the effects of the PP1MEM cation on the coordination number of TFSA anion to Li ion as follows. PP1MEM cation in the electrolyte attracts Li ion interacting TFSA anion through the two oxygen atoms in the cation structure by an electrostatic interaction between the positively charged Li ion and the negatively charged oxygen atoms. After that, a complex consisted of PP1MEM cation and LiTFSA is formed, and the complex is surrounded by an additional TFSA anion for a charge compensation. On the other hand, alkyl group of PP16 cation has no electron-withdrawing nature, and thereby permit at least more than two TFSA anions to coordinate Li ion. This appears to be a reason why the coordination number of TFSA anions to Li ion in PP1MEM-TFSA is smaller than that in PP16-TFSA. When an negative electrode is charged to provide capacity, the cations of ionic liquids are accumulated on the electrode surface, and the $[Li(TFSA)_x]^{1-x}$ exists opposite the cations in Helmholtz layer. The symbol "x" denotes coordination number, and generally results in "2". Desolvation of $[Li(TFSA)_x]^{1-x}$ occurs at the electrode−electrolyte interface before Li-insertion into Si. The desolvation process is impeded by strongly electrostatic interaction between Li ion and TFSA anions in comparison with organic electrolytes system, which limits charge−discharge capacities in the ionic liquid electrolytes system. In consequence, the capacities become smaller with increasing coordination number due to its slow kinetics, as observed in PP16-TFSA. It was revealed that PP1MEM cation played a role reducing the interaction between Li ion and TFSA anions, and the coordination number was less than two. The decrease in the number led to significant increase in capacities of Si electrode. It was demonstrated that PP1MEM cation enhanced not only Li-ion transfer at the electrode−electrolyte interface but also the initial charge−discharge capacities of Si electrode.

Figure 6 represents a dependence of discharge (Li-extraction) capacities and coulombic efficiencies on cycle numbers for Si electrodes in the piperidinium-based ionic liquid electrolytes. For comparison, the performance in PC was also plotted in this figure. Although Si electrode in PC showed the high discharge capacity of 3060 mA h g^{-1} at the first cycle, the capacity was quickly decreased to 110 mA h g^{-1} by 100th cycle, resulting in a very poor cycle performance. The significant capacity decay is attributed to a disintegration of Si electrode caused by a stress generated during alloying/dealloying reaction of Si with Li. Although the coulombic efficiency of the electrode in PC was temporarily increased to 99% at the 10th cycle, the efficiency was decreased to 92% at the 33th cycle. The decline results from the disintegration such as the peeling of the active material from the current collector. On the other hand, The Si electrode in PP1MEM-TFSA showed the first coulombic efficiency of 83%, which is larger than that obtained from PP16-TFSA (68%). These irreversible capacities come from the decomposition of electrolytes to form a surface layer on the anode. It was reported that surface layer derived from TFSA-based ionic liquids is composed of lithium fluoride (LiF), lithium carbonate (Li_2CO_3), lithium sulfate (Li_2SO_4), and lithium sulfite (Li_2SO_3).[23] The Si electrodes in PP1MEM-TSFA and PP16-TFSA gave better cyclability: the capacities of over 1000 mA h g^{-1} were maintained even after 100th cycle. We were able to confirm the excellent reproducibility of anode performances in each case, and an advantage of utilization of ionic liquid electrolyte are obvious throughout the 100 cycles test (Figure 7). Although the capacity in PP1MEM-TFSA was higher than that in PP16-TFSA until 40th cycle, behaviors of cycle performances in each electrolytes overlapped after 50th cycle. From range of Li-insertion plateau between 0.005 and 0.120 V vs. Li/Li$^+$, the initial lithiation capacities based on Li−Si alloying reaction in PP1MEM-TFSA and PP16-TFSA can be estimated to be about 2800 mA h g^{-1} and 2070 mA h g^{-1}, respectively. These capacities are basically close to the theoretical capacity of $Li_{13}Si_4$ (3110 mA h g^{-1}) and Li_7Si_3 (2230 mA h g^{-1}), and the volumetric change ratios per Si atom from Si to $Li_{13}Si_4$ and Li_7Si_3 correspond to 340% and 260%.[51]

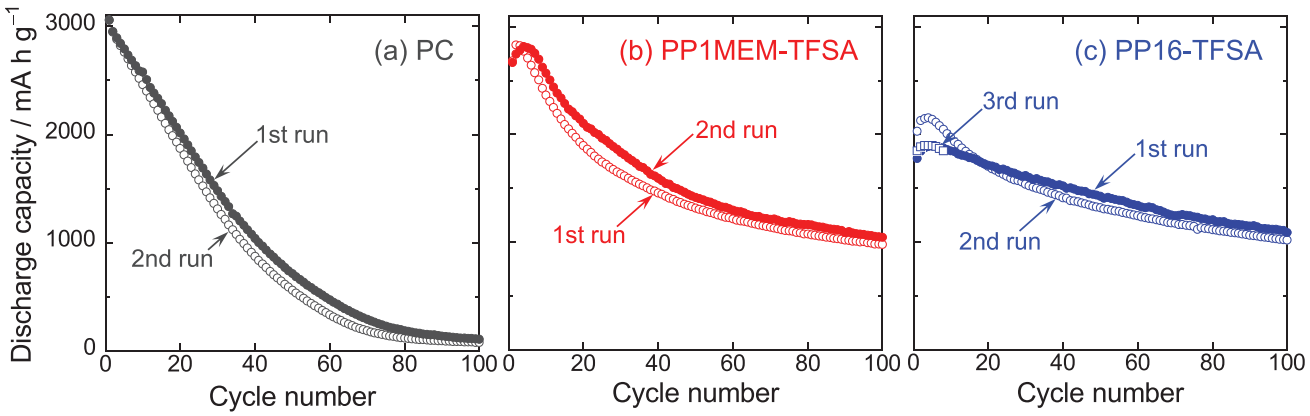

Figure 7. Results of reproductive experiment for cycling performances of Si electrode in (a) PC, (b) PP1MEM-TFSA, and (c) PP16-TFSA. To evaluate reproducibility, the performances were measured for another electrodes as 2nd or 3rd run sample.

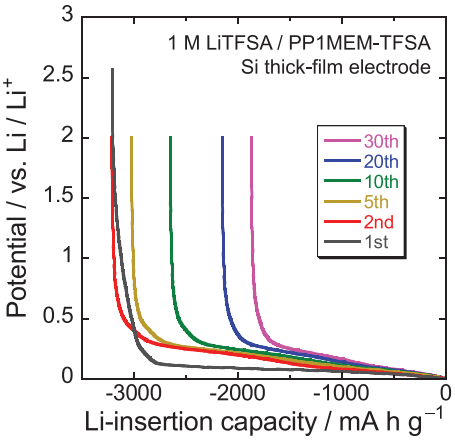

Figure 8. Charge (Li-insertion) profiles during the initial 30 cycles for Si thick-film electrode in PP1MEM-TFSA.

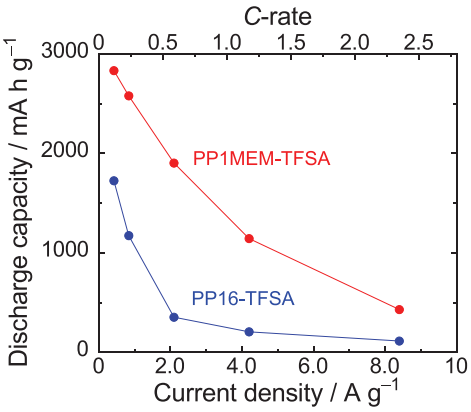

Figure 10. Rate capability of Si electrodes in PP1MEM-TFSA and PP16-TFSA at various current rates from 0.42 to 8.4 A g^{-1}.

The Si in PP1MEM-TFSA expands by the difference in the volumetric change ratio, which results in a generation of a larger strain in the active material. In addition, we could not confirm an additional potential plateau or a shoulder related to the electrolyte decomposition with the exception of lithiation reaction from the charge profiles after second cycle (Figure 8). It is suggested that the lower efficiency in PP1MEM-TFSA is not relevant to the formation of surface layer such as solid electrolyte interphase (SEI). From the above, the reason for the capacity decay in the initial 40th cycle in PP1MEM-TFSA is considered to be due to the greater breakup of Si electrode. It was noteworthy that the Si electrode in PP1MEM-TFSA exhibited the initial capacity comparable to that in PC but still attained the high capacity of 1050 mA h g^{-1} at the 100th cycle. The essential difference in electrode performances obtained from the ionic liquid electrolyte and the organic electrolyte will be reported in future article.

Figure 9 displays FE-SEM images of the Si electrodes before and after 100th charge−discharge cycle in PC, PP1MEM-TFSA, and PP16-TFSA. The as prepared Si electrode showed a comparatively smooth surface as shown in Figure 9a. After cycling in PC, we can clearly observe the disintegration of Si electrode related to the rapid capacity fading (Figure 9b). On the contrary, the disintegration of Si electrodes were relatively suppressed in the cases of using the ionic liquid electrolytes though there were changes in surface morphology such as partial breakup and the formation of cracks (see Figures 9c and 9d). Among them, the degree of disintegration of Si electrode in PP1MEM-TFSA was larger than that in PP16-TFSA, which also means that the capacity decay of Si electrode during the initial 40th cycle in PP1MEM-TFSA originates from the disintegration of the electrode.

Figure 10 illustrates a rate performance of Si electrodes in ionic liquid electrolytes. The characteristic of PP1MEM cation that reduces the interaction between Li ions and TFSA anions is expected to upgrade an anode performance of Si electrodes at high-rate charge−discharge condition. The rate capability was evaluated at various current densities from 420 (0.12 *C*) to 8400 mA g^{-1} (1.2 *C*). The Si electrode in PP16-TFSA showed a rapid capacity decay with increasing current

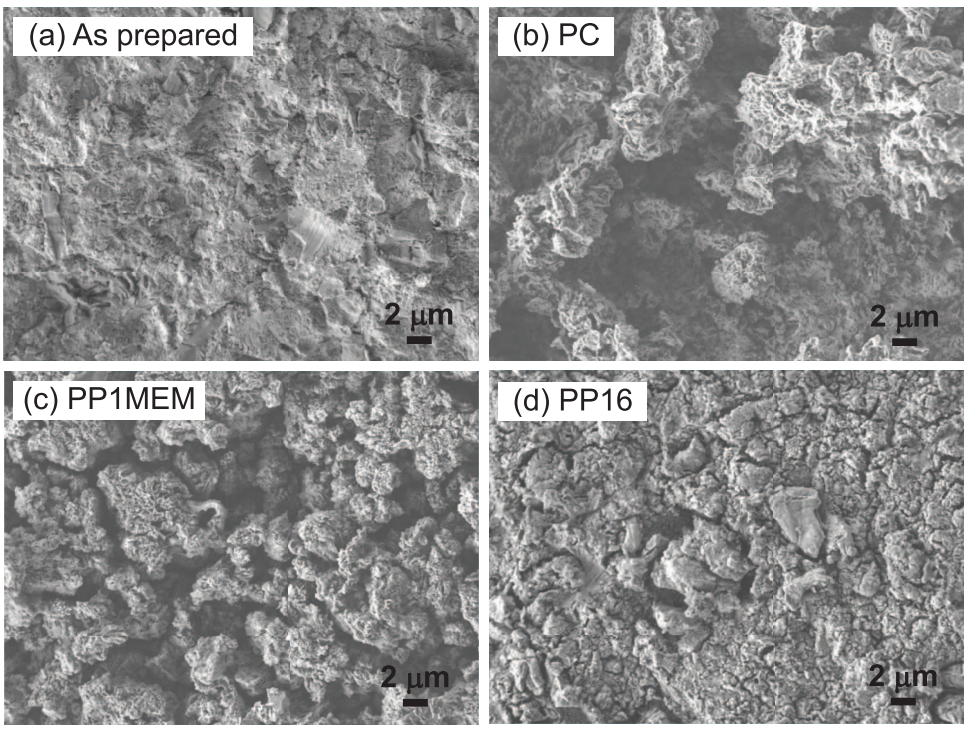

Figure 9. FE-SEM images of Si thick-film electrodes (a) as prepared and after 100th charge–discharge cycle in (b) PC, (c) PP1MEM-TFSA, and (d) PP16-TFSA.

density: the capacity at 1.2 *C* was 210 mA h g^{-1}, which corresponds to about one-tenth of the capacity at 0.12 *C*. This poor rate capability results from slow kinetics of interfacial Li-ion transfer between the electrode and the electrolyte. On the other hand, PP1MEM-TFSA delivered a comparatively high discharge capacity of 1150 mA h g^{-1} even at a high current density of 4200 mA g^{-1} (1.2 *C*), indicating that the Li-ion transfer was remarkably improved by PP1MEM cation. An application of PP1MEM-TFSA to Si-based composite electrodes that we have demonstrated their superiority expects that the electrode performance can be further improved.

Conclusions

The Si thick-film electrodes were prepared by a gas-deposition method, and the influences of cation structure of ionic liquids on anode properties of Si electrodes were investigated from the viewpoint of interaction between Li ion and TFSA anions. The Si electrode in ionic liquid consisted of PP1MEM cation having electron-donating group and TFSA anion exhibited the high discharge capacity of 2670 mA h g^{-1} at the first cycle, which is larger than that in PP16-TFSA by ca. 900 mA h g^{-1}. Raman analysis and EIS measurements revealed that PP1MEM cation played a role reducing the interaction between Li ion and TFSA anions, and that Li-ion transfer at the interface between electrode and electrolyte was improved compared with PP16-TFSA. The excellent cycle performances, discharge capacities of over 1000 mA h g^{-1} at 100th cycle, were attained in both the ionic liquid electrolytes whereas the Si electrode in PC showed the capacity of 110 mA h g^{-1}. Additionally, the improved interfacial Li-ion transfer, the smooth Li-insertion into Si in PP1MEM-TFSA led to a good high-rate performance: the capacity of 1150 mA h g^{-1} at relatively a high current density of 4200 mA g^{-1} (1.2 *C*) was achieved. These results indicates that the introduction of ether functional group into cation structure is effective strategy for enhancement of anode performance of Si electrodes.

Acknowledgments

M. Shimizu thanks Japan Society for the Promotion of Science (JSPS) for research fellowship (No. 2611485). This work has been supported by a grant-in-Aid for Young Scientists (B) (No. 25810141) from Scientific Research of Ministry of Education, Culture, Sports, Science and Technology (MEXT) of Japan. The authors thank A. Sato for synthesis of ionic liquids.

References

1. C. J. Wen and R. A. Huggins, *J. Solid State Chem.*, **37**, 271 (1981).
2. M. N. Obrovac and L. Christensen, *Electrochem. Solid-State Lett.*, **7**, A93 (2004).
3. T. D. Hatchard and J. R. Dahn, *J. Electrochem. Soc.*, **151**, A838 (2004).
4. M. N. Obrovac and L. J. Krause, *J. Electrochem. Soc.*, **154**, A103 (2007).
5. N. Ding, J. Xu, Y. X. Yao, G. Wegner, X. Fang, C. H. Chen, and I. Lieberwirth, *Solid State Ionics*, **180**, 222 (2009).
6. J. Xie, N. Imanishi, T. Zhang, A. Hirano, Y. Takeda, and O. Yamamoto, *Mater. Chem. Phys.*, **120**, 421 (2010).
7. M. Thakur, S. L. Sinsabaugh, M. J. Isaacson, M. S. Wong, and S. L. Biswal, *Sci. Rep.*, **2**, 795 (2012).
8. A. Magasinski, P. Dixon, B. Hertzberg, A. Kvit, J. Ayala, and G. Yushin, *Nat. Mater.*, **9**, 353 (2010).
9. Y. Chen, S. Zeng, J. Qian, Y. Wang, Y. Cao, H. Yang, and X. Ai, *ACS Appl. Mater. Interfaces*, **6**, 3508 (2014).
10. C. Wang, H. Wu, Z. Chen, M. T. McDowell, Y. Cui, and Z. Bao, *Nature Chem.*, **5**, 1042 (2013).
11. H. Sakaguchi, T. Iida, M. Itoh, N. Shibamura, and T. Hirono, *IOP Conf. Series: Mater. Sci. Eng.*, **1**, 012030 (2009).
12. H. Usui, K. Meabara, K. Nakai, and H. Sakaguchi, *Int. J. Electrochem. Sci.*, **6**, 2246 (2011).
13. H. Usui, M. Shibata, K. Nakai, and H. Sakaguchi, *J. Power Sources*, **196**, 2143 (2011).
14. H. Usui, N. Uchida, and H. Sakaguchi, *Electrochemistry*, **80**, 737 (2012).
15. M. Ishikawa, T. Sugimoto, M. Kikuta, E. Ishiko, and M. Kono, *J. Power Sources*, **162**, 658 (2006).
16. H. Sano, H. Sakaebe, and H. Matsumoto, *J. Electrochem. Soc.*, **158**, A316 (2011).
17. S. Seki, Y. Ohno, H. Miyashiro, Y. Kobayashi, A. Usami, Y. Mita, N. Terada, K. Hayamizu, S. Tsuzuki, and M. Watanabe, *J. Electrochem. Soc.*, **155**, A421 (2008).
18. M. Egashira, A. Kanetomo, N. Yoshimoto, and M. Morita, *J. Power Sources*, **196**, 6419 (2011).
19. V. Baranchugov, E. Markevich, E. Pollak, G. Salitra, and D. Aurbach, *Electrochem. Commun.*, **9**, 796 (2007).
20. C. C. Nguyen and S.-W. Song, *Electrochem. Commun.*, **12**, 1593 (2010).
21. T. Sugimoto, Y. Atsumi, M. Kono, M. Kikuta, E. Ishiko, M. Yamagata, and M. Ishikawa, *J. Power Sources*, **195**, 6153 (2010).
22. N. Yabuuchi, K. Shimomura, Y. Shimbe, T. Ozeki, J.-Y. Son, H. Oji, Y. Katayama, T. Miura, and S. Komaba, *Adv. Energy Mater.*, **1**, 759 (2011).
23. J.-W. Song, C. C. Nguyen, and S.-W. Song, *RSC Adv.*, **2**, 2003 (2012).
24. C. C. Nguyen, S.-W. Woo, and S.-W. Song, *J. Phys. Chem. C*, **116**, 14764 (2012).
25. J.-A. Choi, D.-W. Kim, Y.-S. Bae, S.-W. Song, S.-H. Hong, and S.-M. Lee, *Electrochim. Acta*, **56**, 9818 (2011).
26. H. Usui, Y. Yamamoto, K. Yoshiyama, T. Itoh, and H. Sakaguchi, *J. Power Sources*, **196**, 3911 (2011).
27. H. Usui, T. Masuda, and H. Sakaguchi, *Chem. Lett.*, **41**, 521 (2012).
28. H. Usui, M. Shimizu, and H. Sakaguchi, *J. Power Sources*, **235**, 29 (2013).
29. J. C. Lassegues, J. Grondin, and D. Talaga, *Phys. Chem. Chem. Phys.*, **8**, 5629 (2006).
30. Y. Umebayashi, T. Mitsugi, S. Fukuda, T. Fujimori, K. Fujii, R. Kanzaki, M. Takeuchi, and S. Ishiguro, *J. Phys. Chem. B*, **111**, 13028 (2007).
31. Y. Umebayashi, S. Mori, K. Fujii, S. Tsuzuki, S. Seki, K. Hayamizu, and S. Ishiguro, *J. Phys. Chem. B*, **114**, 6513 (2010).
32. M. Yamagata, N. Nishigaki, S. Nishishita, Y. Matsui, T. Sugimoto, M. Kikuta, T. Higashizaki, M. Kono, and M. Ishikawa, *Electrochim. Acta*, **110**, 181 (2013).
33. Y. Katayama, R. Fukui, and T. Miura, *J. Electrochem. Soc.*, **154**, D534 (2007).
34. Y. Yamada, Y. Iriyama, T. Abe, and Z. Ogumi, *J. Electrochem. Soc.*, **157**, A26 (2010).
35. B. Baek, S. Lee, and C. Jung, *Int. J. Electrochem. Sci.*, **6**, 6220 (2011).
36. Y. Wang, K. Zaghib, A. Guerfi, F.F.C. Bazito, R.M. Torresi, and J.R. Dahn, *Electrochimica Acta*, **52**, 6346 (2007).
37. H. Sakaguchi, T. Toda, Y. Nagao, and T. Esaka, *Electrochem. Solid-State Lett.*, **10**, J146 (2007).
38. M. Shimizu, H. Usui, and H. Sakaguchi, *J. Power Sources*, **248**, 378 (2014).
39. Y. Abe, K. Yoshiyama, Y. Yagi, S. Hayase, M. Kawatsura, and T. Itoh, *Green Chem.*, **12**, 1976 (2010).
40. H.-B. Han, K. Liu, S.-W. Feng, S.-S. Zhou, W.-F. Feng, J. Nie, H. Li, X.-J. Huang, H. Matsumoto, M. Armand, and Z.-B. Zhou, *Electrochim. Acta*, **55**, 7134 (2010).
41. J. Reiter, E. Paillard, L. Grande, M. Winter, and S. Passerini, *Electrochim. Acta*, **91**, 101 (2013).
42. K. Tsunashima, A. Kawabata, M. Matsumiya, S. Kodama, R. Enomoto, M. Sugiya, and Y. Kunugi, *Electrochem. Commun.*, **13**, 178 (2011).
43. J.-T. Li, J. Swiatowska, A. Seyeux, L. Huang, V. Maurice, S.-G. Sun, and P. Marcus, *J. Power Sources*, **195**, 8251 (2010).
44. I. Rey, P. Johansson, J. Lindgren, J. C. Lassègues, J. Grondin, and L. Servant, *J. Phys. Chem. A*, **102**, 3249 (1998).
45. S. P. Gejji, C. H. Suresh, K. Babu, and S. R. Gadre, *J. Phys. Chem. A*, **103**, 7474 (1999).
46. M. Herstedt, M. Smirnov, P. Johansson, M. Chami, J. Grondin, L. Servant, and J. C. Lassègues, *J. Raman Spectrosc.*, **36**, 762 (2005).
47. M. Kunze, S. Jeong, E. Paillard, M. Schönhoff, M. Winter, and S. Passerini, *Adv. Energy Mater.*, **1**, 274 (2011).
48. M. Kunze, E. Paillard, S. Jeong, G. B. Appetecchi, M. Schoenhoff, M. Winter, and S. Passerini, *J. Phys. Chem. C*, **115**, 19431 (2011).
49. S. Tsuzuki, H. Tokuda, K. Hayamizu, and M. Watanabe, *J. Phys. Chem. B*, **109**, 16474 (2005).
50. S. Tsuzuki, K. Hayamizu, S. Seki, Y. Ohno, Y. Kobayashi, and H. Miyashiro, *J. Phys. Chem. B*, **112**, 9914 (2008).
51. M. K. Datta and P. N. Kumta, *J. Power Sources*, **194**, 1043 (2009).